Numerical and experimental investigation of the efficiency of Classified Cycling's Powershift hub

Bart Blockmans[1,], Dries Ketelslegers[1], Thomas Valero[1], Roëll van Druten[1]

[1] Classified Cycling, Damplein 23, 2060 Antwerp, Belgium

Abstract. Classified Cycling's Powershift Technology is a wireless shifting device that replaces traditional two-gear (2x) front derailleur-based shifting systems by an epicyclic gearing system integrated into the bicycle's rear wheel hub. In doing so, the technology enables instant shifting under full load for both road, gravel and mountain bike cycling, while safeguarding competitive weight and drivetrain efficiency. Although epicyclic transmissions have been extensively used in automotive, aerospace and wind energy applications for their high efficiencies and power densities, several design considerations were taken into account to ensure maximal efficiency of the Powershift Technology. This article investigates the impact of these design choices on the transmission efficiency of the Powershift hub. Using advanced numerical simulations and measurements conducted on a specifically designed efficiency measurement test rig, the Powershift hub efficiency is shown to rival or even surpass that of conventional competitive bicycle transmissions.

---

1. Introduction

Epicyclic or planetary gear transmissions have since long been applied in the automotive, aerospace and wind energy industries due to their high torque-to-weight ratio, low lateral reaction forces, and small power losses. Both in experimental testing and numerical simulation, planetary gear train efficiencies of 99% and more have routinely been recorded in automotive [1], helicopter [2], and wind turbine [3] gearboxes. Even long before their widespread industrial usage, epicyclic gears appeared in tricycle and bicycle hubs [4], although it was not until the 1990s that multi-speed hubs of the likes of Sturmey-Archer [5] and Rohloff [6] started to replace the classical derailleur-based shifting mechanisms as more reliable alternatives. With reliability and long service life as their primary concern, multi-speed hub efficiency has been reported to drop slightly below that of purely derailleur-based systems [7]; however, efficiencies of 98.5% and above have been recorded on numerous occasions in epicyclic hubs consisting of up to three consecutive planetary gear stages [8][9].

Classified Cycling's Powershift Technology is a wireless shifting device that replaces traditional two-gear (2x) front derailleur-based shifting systems by a single-stage 2-speed epicyclic transmission integrated into the bicycle's rear wheel hub (see Figure 1). By combining their planetary hub with a classical rear derailleur and cassette, Classified's hybrid shifting technology enables instant shifting under full load from the large to the virtual small chainring, while safeguarding competitive weight and overall drivetrain efficiency. In order to minimize drivetrain losses, engineers at Classified Cycling exploited several decades of automotive transmission design experience to develop a bicycle drivetrain that holds the premise of being amongst the most efficient on the market. In this article, this premise will be investigated through numerical and experimental analyses of the efficiency of the Powershift Technology.

The remainder of this article is organized as follows. In Section 2, the main operating principles of the Powershift hub are explained so as to provide a sufficient basis for understanding the technical sections of this article. Section 3 presents a numerical model of the power losses occurring in the Powershift hub, which is largely developed using physics-based models so as to minimize the reliance on parameter identification and maximize the model's predictive capabilities. In Section 4 an accuracy analysis of Classified Cycling's tailor-made hub efficiency test rig is given, followed in Section 5 by hub efficiency measurements conducted in both hub ratios and at various operating conditions. Finally, Section 6 summarizes the main findings of this investigation.

Figure 1. Exploded view of Classified Cycling's Powershift Technology hub.

2. Operating principles of the Powershift hub

The powershift hub is a 2-speed epicyclic hub that uses a single planetary stage to accomplish two speed ratios: 1 and 0.686, the latter being roughly equal to the tooth ratio of a conventional 2x setup having e.g. 52 or 53 teeth on the large chainring and 36 teeth on the small chainring. A simplified representation of the hub's planetary gear system is shown in Figure 2. The annulus or ring wheel is connected to the bicycle's cassette that converts chain tension into input torque, whereas the planet carrier is connected to the wheels which convert the hub's output torque into bicycle propulsive force. The configuration of the planetary gear system depends on the selected transmission ratio: in the 1:1 ratio, the ring gear and planet carrier are rigidly linked to each other, causing the planetary gear set to rotate as a single unit with no relative motion between the components. In the 0.686 ratio, the ring and planet carrier can rotate freely with respect to each other while a one-way bearing holds the sun gear in place. This causes the six planet gears to engage with the ring and sun gears, thereby establishing the 0.686 ratio between ring gear and planet carrier displacements, while the torque on the stationary sun gear is supported by the axle and the bike frame.

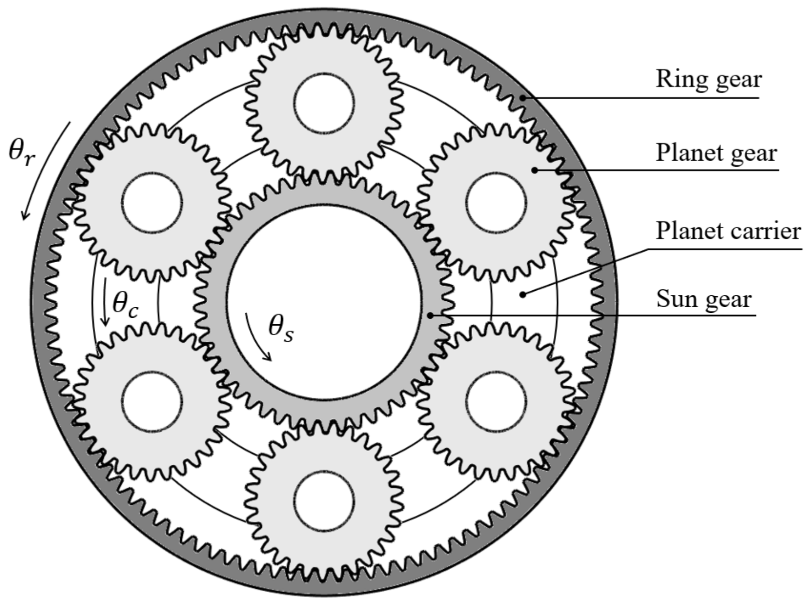

Figure 2. Simplified representation of the Powershift hub planetary gear system.

The fundamental equation describing the kinematics of planetary gears is Willis equation [10], which can be written as follows:

$$\theta_r z_r = \theta_c \cdot (z_r + z_s) - \theta_s z_s \tag{1}$$

where θ refers to angular displacement, z denotes the number of teeth, and the subscripts r, c and s refer to the ring gear, planet carrier, and sun gear, respectively. From the above equation, the following two equations involving the planet gear displacements θ_p are obtained:

$$(z_s + z_p)\theta_c = \theta_s z_s + \theta_p z_p \qquad (z_r - z_p)\theta_c = \theta_r z_r - \theta_p z_p \tag{2}$$

As the angular displacement of the sun gear is fixed in the 0.686 ratio ($\theta_s = 0$ in Eq. 1), the ratio u_{PS} between output angular displacement θ_c and input angular displacement θ_r can be expressed as follows:

$$u_{PS} = \frac{\theta_c}{\theta_r} = \frac{z_r}{(z_r + z_s)} \approx 0.686 \tag{3}$$

While there are many ways to obtain a reduction ratio using planetary gears, the sun-locked configuration in the Powershift hub was deliberately selected due to its advantageous theoretical efficiency. This has been extensively studied in literature using a variety of analytical, graphical and numerical approaches (see e.g. [12]). For the specific case of the sun-locked single-stage transmission, the following theoretical efficiency equation can be derived [10]:

$$\eta_{th} = \frac{(z_r/z_s) + \eta_0}{(z_r/z_s) + 1} = \frac{u_{rs} + \eta_0}{u_{rs} + 1} \qquad \text{where} \qquad \eta_0 = \eta_{pr}\eta_{sp} \tag{4}$$

where η_{th} is the total planetary gear efficiency, η_0 is the total gear mesh efficiency and η_{pr} and η_{sp} are the mesh efficiencies of the planet-ring and sun-planet pairs, respectively. Note that this equation is based on an ideal kinematic analysis of a planetary gear stage in which the only power losses considered are the gear meshing losses. A simple expression for spur gear mesh efficiency is given by [13] as:

$$\eta_{ij} = 1 - \pi\mu_{ij}\left(\frac{1}{z_i} + \frac{1}{z_j}\right) \tag{5}$$

where the subscripts i and j refer to the pinion and gear of the considered gear pair, and μ is the coefficient of friction. For more advanced expressions of spur gear mesh efficiency, see e.g. [14]. Substitution of the above equation into Eq. 4 allows one to plot the theoretical efficiency of the planetary transmission in function of the friction coefficient, as is shown in Figure 3 for the Powershift hub. Note that the overall theoretical efficiency η_{th} in the sun-locked configuration (i.e. the 0.686 ratio) is always higher than the individual mesh efficiencies. For lubricated gear pairs, the instantaneous friction coefficient can drop significantly below 0.05 [15], resulting in theoretical efficiencies of 99.5% and more.

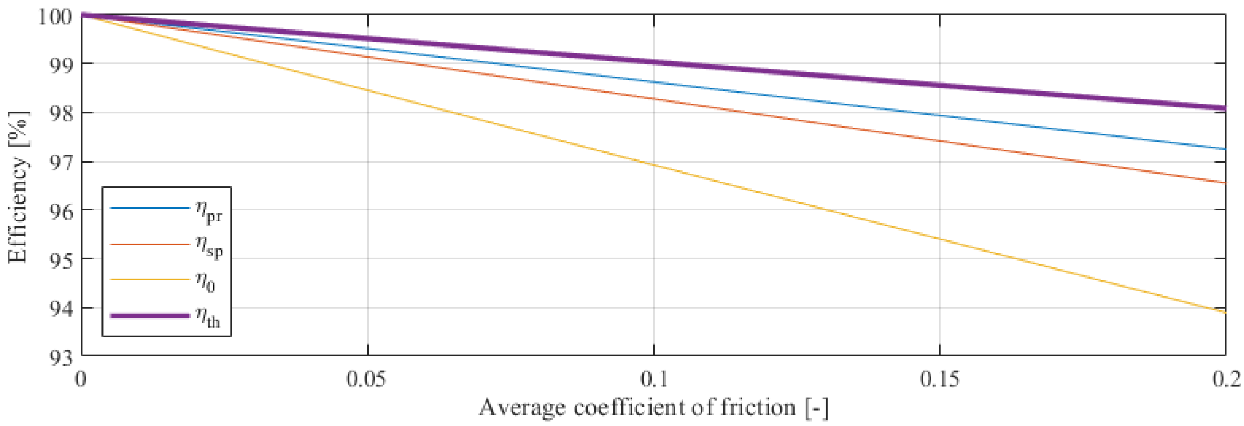

Figure 3. Theoretical efficiency of the sun-locked planetary gear stage in function of coefficient of friction.

Besides power losses in the gear contacts, which are the only losses considered thus far, bearings represent an additional source of power loss in planetary gear systems. In the Powershift hub, the planet carrier (and thus the bicycle's rear wheel) is supported by two deep-groove ball bearings, and the ring gear (and thus the bicycle's cassette) is also supported by two deep-groove ball bearings. These bearings are similar to the main bearings in conventional hubs, albeit that in the 1:1 ratio the Powershift hub operates with one bearing less as one of the bearings is short-circuited and thus does not contribute to the overall power loss. The same holds for the needle bearings that support the planet gears in the Powershift hub. In the next section, a numerical model is developed to accurately predict the power losses in the Powershift hub in both the 1:1 and 0.686 ratios.

3. Numerical prediction of the power losses in the Powershift hub

The power losses in any transmission can be categorized into two main groups, see Figure 4. Load-dependent power losses – also referred to as mechanical or frictional losses – are due to the sliding and rolling actions of the lubricated contact surfaces at the gear mesh and bearing contacts. They are dependent on the load transmitted through the planetary gear system. Load-independent losses – sometimes referred to as spin losses – are attributed to the losses in the gear system under no-load, and consist of drag losses, oil pocketing (or squeezing) losses, viscous losses in the bearings and bearing seal losses [16].

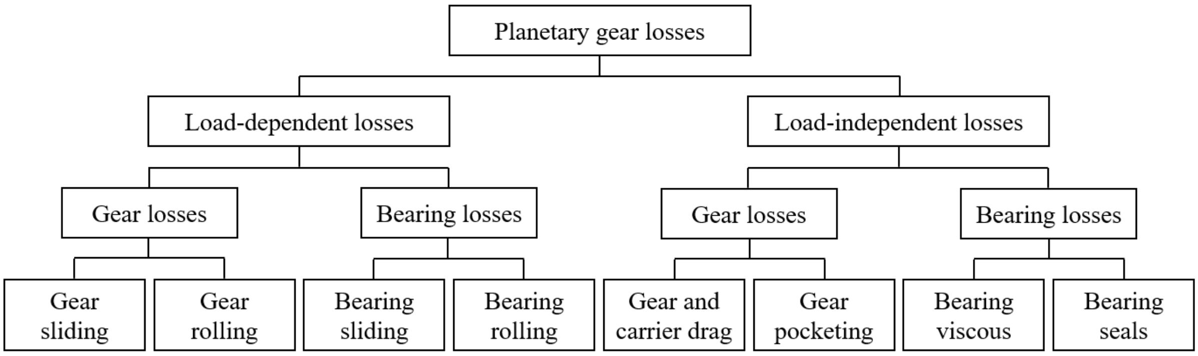

Figure 4. Classification of power losses in a planetary gear stage.

3.1 Load-dependent power losses in the Powershift hub

Loaded tooth contact analysis. In gears, load-dependent power losses typically depend on the normal contact forces acting between mating tooth flanks, whereas in bearings the resultant radial and axial forces on the bearing ultimately determine the load-dependent losses. A detailed power loss analysis thus requires a loaded contact analysis of the system under consideration. In the presented investigation, a three-dimensional semi-analytical model based on thin-slicing was implemented to allow for accurate load distribution assessment at a reasonable computational cost [17]. For power loss computations, the components of the planetary gear train are assumed to be perfectly aligned with bearings represented by ideal revolute joints. The contact model consists of three main components: the analytical computation of the contact stiffness of the gears, the analytical computation of the individual slice compressions, and finally the numerical computation of the resulting contact force distribution.

The contact stiffnesses of the ring, sun and planet gears are computed based on an extension of the work of Weber and Banascheck [18] (see [17] for an in-depth discussion of these extensions), who use linear elasticity theory to derive integral expressions for the various components of the global compliance of involute gears, and who complement these linear compliances with a nonlinear local contact compliance derived from Hertzian contact theory (see also [19]). For the computation of the individual slice compressions δ_i, involute gear contact kinematics (see e.g. [20]) yields the following expression with reference to Figure 5:

$$\delta_i = |T_1Y_1| \pm |T_2Y_2| - |T_1T_2| - \delta_{mod,p} - \delta_{mod,g} \tag{6}$$

In this equation, the distances $|T_1Y_1|$ and $|T_2Y_2|$ are the respective radii of curvature at the contact points, which can be expressed in terms of the base radius and the roll angle of the respective gears and thus depend on the angular configuration of the gear pair. Furthermore, the distance $|T_1T_2|$ depends on the gear pair's center distance and working pressure angle (and is thus fixed in the case of perfectly aligned and rigidly supported gears), and $\delta_{mod,p}$ and $\delta_{mod,g}$ represent the normal microgeometry modifications of the pinion and gear. The minus sign in the above equation is to be used in the case of external-internal gear contact, as is the case in the planet-ring contacts. Given the angular configuration of any gear pair, the individual slice compressions for all teeth in contact can be evaluated using the above equation, and the slice contact forces can be computed by solving the following equation:

$$\{\boldsymbol{\delta}\} - [\boldsymbol{C}]\{\boldsymbol{f}_c\} = \{\boldsymbol{0}\} \tag{7}$$

where $\boldsymbol{\delta}$ is the vector of slice compressions, $\boldsymbol{f}_c$ is the vector of normal slice contact forces, and $\boldsymbol{C}$ is the so-called compliance matrix of all slices in contact, which is assembled based on the contact compliances and possible coupling compliances corresponding to the contact locations (see [17] for a detailed explanation of how to assemble this matrix). Note that this equation represents a Non-Linear Complementarity Problem (NLCP) that needs to be solved iteratively for $\boldsymbol{f}_c$ so as to avoid unphysical contact forces. Once the vector of normal contact forces is determined, the resultant contact force $\boldsymbol{Q}_c$ acting on the gear center can be computed by projection and summation of all individual normal slice contact forces $f_{c,i}$:

$$\boldsymbol{Q}_c = \begin{Bmatrix} \boldsymbol{F}_c \\ \boldsymbol{M}_c \end{Bmatrix} = \begin{Bmatrix} \{F_{c,x}, F_{c,y}, F_{c,z}\}^T \\ \{M_{c,x}, M_{c,y}, M_{c,z}\}^T \end{Bmatrix} = \sum_{i=1}^{N_s} f_{c,i} \begin{Bmatrix} \boldsymbol{n}_{c,i} \\ \boldsymbol{r}_{c,i} \times \boldsymbol{n}_{c,i} \end{Bmatrix} \tag{8}$$

where $\boldsymbol{n}_{c,i}$ represents the local normal to the contact point at the i-th slice, $\boldsymbol{r}_{c,i}$ is the position vector of this contact point, and N_s is the number of slices in contact. The total reaction forces on the ring, sun and planet gears and by the planet carrier are obtained as:

$$\boldsymbol{Q}_c^r = -\sum_{j=1}^{N_p} \boldsymbol{Q}_c^{pr,j} \qquad \boldsymbol{Q}_c^s = \sum_{j=1}^{N_p} \boldsymbol{Q}_c^{sp,j} \qquad \boldsymbol{Q}_c^j = \boldsymbol{Q}_c^{pr,j} - \boldsymbol{Q}_c^{sp,j} \qquad \boldsymbol{Q}_c^c = \sum_{j=1}^{N_p} \begin{Bmatrix} \boldsymbol{F}_c^j \\ \boldsymbol{M}_c^j + \boldsymbol{r}_{pin}^j \times \boldsymbol{F}_c^j \end{Bmatrix} \tag{9}$$

where N_p is the number of planet gears and $\boldsymbol{r}_{pin}^j$ is the position vector of the j-th planet carrier pin. Having obtained the reaction forces at all planetary gear components, the three-dimensional reaction forces in the bearings of the Powershift hub can be determined from static equilibrium considerations (see e.g. [22]).

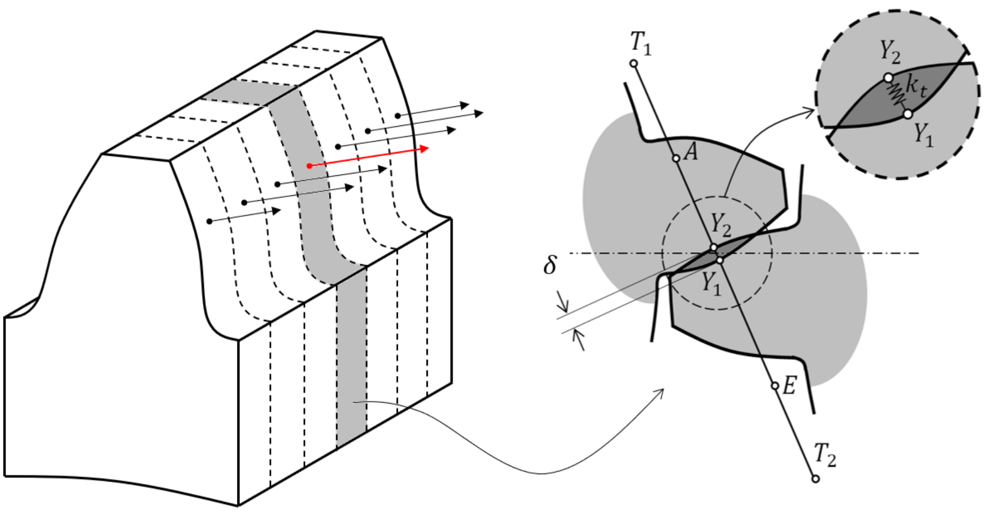

Figure 5. Analytical computation of the thin-slice contact forces using involute gear contact kinematics (adapted from [21]).

Power loss computation of grease-lubricated gears and bearings. In the subsequent sections, a numerical model to predict power losses in the Powershift hub will be described. These losses depend to a high extend on the lubricant applied to the internal components of the hub [23], which in the case of the Powershift hub is a grease, i.e. a combination of a base oil (80-90%) and a thickener which retains the oil through capillary action. The literature on grease-lubricated gear and bearing power losses is scarce, which can be attributed to the complexity of the rheological behavior of greases [24]. Power losses of oil-lubricated gears and bearings, instead, are extensively dealt with in scientific literature, resulting in a multitude of experimentally validated analytical and semi-empirical models for the prediction of load-dependent and load-independent power losses. Despite the rheological differences between liquid lubricants and greases, the power loss mechanisms of both lubricants are highly similar and can often be quantified using similar models [25]. This is particularly true for load-dependent power losses, which essentially depend on friction coefficients that can equally well be determined for grease-lubricated contact surfaces [26]. For the prediction of load-independent drag losses, most numerical models available in literature assume the availability of a meaningful 'submerged height' parameter, which is difficult to define for grease-lubricated gears and bearings. While several researchers have opted to omit these losses for grease-lubricated gears or bearings [27], this strategy is not adopted in the current work. Instead, as the presented loss model aims to provide lower bounds on the attainable efficiency of the design to steer design considerations, all power losses relevant to oil-lubricated gears and bearings are included in the model, where full submergence is assumed in the computation of drag losses and equivalent rheological parameters are used to characterize the grease.

Frictional losses in the gear contacts. Frictional losses in gears are due to sliding and rolling actions of the interacting components and lubricant film in the gear mesh. The instantaneous power loss due to gear friction of a single planetary stage $P_{f,gear}$ can be written as follows:

$$P_{f,g} = \sum_{j=1}^{N_p} \left[\left(S_{g,j}^{sp} + R_{g,j}^{sp} \right) + \left(S_{g,j}^{pr} + R_{g,j}^{pr} \right) \right] = \sum_{j=1}^{N_p} \sum_{i=1}^{N_s} \left[\left(S_{g,ij}^{sp} + R_{g,ij}^{sp} \right) + \left(S_{g,ij}^{pr} + R_{g,ij}^{pr} \right) \right] \tag{10}$$

where N_p is the number of planet gears, S_g and R_g refer to the gear sliding and rolling power losses, and the superscripts sp and pr refer to the sun-planet and the planet-ring pairs. The sliding power loss corresponding to a single slice in contact can be expressed as follows:

$$S_{g,i} = \mu_i f_{c,i} \left(u_{p,i} - u_{g,i} \right) = \mu_i f_{c,i} V_{s,i} \tag{11}$$

where μ_i is the local friction coefficient, $V_{s,i}$ is the local sliding velocity, and $u_{p,i}$ and $u_{g,i}$ are the local surface velocities of the pinion and gear. The latter are obtained by multiplication of the local radii of curvature with the gears' angular velocities, taking into account the rotation of the planet carrier (see e.g. [16]). The coefficient of friction μ_i is computed using the formula derived by Xu et al. [24] based on a regression analysis of around 10,000 numerical Elasto-Hydro-dynamic Lubrication (EHL) simulations, and is expressed in terms of the inlet temperature, lubricant viscosity, slide-to-roll ratio $SR = V_{s,i}/V_{e,i}$, radius of curvature, entraining velocity, Hertzian contact pressure, and surface roughness.

The rolling power loss corresponding to a single slice in contact can be expressed as follows:

$$R_{g,i} = f_{r,i} \left(u_{p,i} + u_{g,i} \right) = 2 f_{r,i} V_{e,i} \tag{12}$$

where $V_{e,i} = 0.5\left(u_{p,i} + u_{g,i} \right)$ is the local entrainment velocity, and $f_{r,i}$ is the isothermal rolling friction force due to lubricant build-up. The latter is computed according to [29] as

$$f_{r,i} = 4.318 \cdot \frac{\rho_{e,i} b_i}{\alpha} \cdot \left(\frac{\alpha \mu_i V_{e,i}}{\rho_{e,i}} \right)^{0.658} \cdot \left(\frac{f_{c,i}}{E_e \rho_{e,i} b_i} \right)^{0.0126} \tag{13}$$

where $\rho_{e,i} = \left(\rho_{p,i}^{-1} + \rho_{g,i}^{-1} \right)^{-1}$ is the equivalent radius of curvature, b_i is the width of the slice, α is the pressure-viscosity coefficient of the lubricant, and $E_e = 2\left(\left(1 - \nu_p^2\right)/E_p + \left(1 - \nu_g^2\right)/E_g \right)^{-1}$ the combined Young's modulus, with ν_p and ν_g the Poisson coefficients of the pinion and gear. The above expression is multiplied by a thermal reduction factor to account for the effect of temperature increases at elevated speed (see [30]).

Frictional losses in the bearing contacts. In order to reduce the computational complexity of the analysis while safeguarding scientific soundness, the SKF friction model [25] is used to compute the bearings' sliding and rolling friction power losses. This model was derived by SKF based on regression analyses of extensive simulation results obtained using SKF's physics-based bearing simulation tools [31]. The instantaneous power loss due to load-dependent bearing friction of the complete Powershift hub $P_{f,b}$ can be written as:

$$P_{f,b} = \sum_{j=1}^{N_m} \left[\left(S_{b,j}^m + R_{b,j}^m \right) \right] + \sum_{j=1}^{N_p} \left[\left(S_{b,j}^p + R_{b,j}^p \right) \right] \tag{14}$$

where N_m is the number of main bearings supporting the hub, S_b and R_b refer to the bearing sliding and rolling power losses, and the superscripts m and p refer to the main and planet bearings, respectively. Note that for the 0.686 ratio, $N_m = 4$ and $N_p = 6$, whereas in the 1:1 ratio $N_m = 3$ and $N_p = 0$. The bearing sliding power losses of deep-groove ball bearings (S_b^m) and needle bearings (S_b^p) are expressed as follows [25]:

$$S_b^m = \mu_b S_1 d_m^{-0.145} \left(F_r^5 + \frac{S_2 d_m^{1.5}}{\sin \alpha_F} F_a^4 \right)^{1/3} \qquad S_b^p = \mu_b (s_1 d_m^{0.9} F_r + d_m F_{ra}) \tag{15}$$

where S_1 and S_2 are bearing geometry constants defined in [25], d_m is the mean bearing diameter, F_r and F_a are the radial and axial forces acting on the bearing (cfr. Eq. 9), and α_F is defined as $\alpha_F = 24.6(F_a/C_0)^{0.24}[°]$, with C_0 the basic static load rating of the bearing. The bearing friction coefficient μ_b depends on the lubrication state, as expressed by the weighting factor ϕ_{bl}:

$$\mu_b = \phi_{bl}\mu_{bl} + (1 - \phi_{bl})\mu_{b,EHL} \qquad \text{where} \qquad \phi_{bl} = \frac{1}{e^{2.6 \cdot 10^{-8}(n\nu)^{1.4} d_m}} \tag{16}$$

where $\mu_{bl} = 0.12$, $\mu_{b,EHL}$ is the sliding friction coefficient in full-film conditions, n is the rotational velocity of the bearing inner ring with respect to the outer ring expressed in rpm, and ν is the actual operating viscosity of the grease. For the planet bearings, the rotational velocity n can be obtained from the hub input (ring) or output (carrier) velocities using the fundamental kinematic planetary gear equations, Eq. 1-2.

The bearing rolling power losses of deep-groove ball bearings (R_b^m) and needle bearings (R_b^p) are expressed as follows [25]:

$$R_b^m = \phi_{ish}\phi_{rs}\mu_b R_1 d_m^{1.96} \left(F_r + \frac{R_2}{\sin \alpha_F} F_a \right)^{0.54} (n\nu)^{0.6} \qquad R_b^p = \phi_{ish}\phi_{rs}\mu_b R_1 d_m^{2.41} F_r^{0.31} (n\nu)^{0.6} \tag{17}$$

where R_1 and R_2 are bearing geometry constants defined in [25]. The factors ϕ_{ish} and ϕ_{rs} account for inlet shear heating and the kinematic replenishment effect and are obtained as follows:

$$\phi_{ish} = \frac{1}{1 + 1.84 \cdot 10^{-9} (n d_m)^{1.28} \nu^{0.64}} \qquad \phi_{rs} = \frac{1}{e^{K_{rs} \nu n (d+D) \sqrt{\frac{K_z}{2(D-d)}}}} \tag{18}$$

where $K_{rs} = 6 \times 10^{-8}$ for grease lubrications, K_z depends on the bearing type (see [25]), d is the bearing bore diameter and D is the bearing outside diameter.

The load-dependent power losses of the Powershift hub can be summarized as follows:

$$P_f = P_{f,g} + P_{f,b} = \sum_{j=1}^{N_p^*} \left[\left(S_{g,j}^{sp} + R_{g,j}^{sp} \right) + \left(S_{g,j}^{pr} + R_{g,j}^{pr} \right) \right] + \sum_{j=1}^{N_m^*} \left[\left(S_{b,j}^m + R_{b,j}^m \right) \right] + \sum_{j=1}^{N_p^*} \left[\left(S_{b,j}^p + R_{b,j}^p \right) \right] \tag{19}$$

where the asterisk symbol is used to denote that for the 0.686 ratio, $N_m = 4$ and $N_p = 6$, whereas in the 1:1 ratio $N_m = 3$ and $N_p = 0$.

3.2 Load-independent power losses in the Powershift hub

Load-independent losses in gears. The load-independent power losses in planetary gears consist of viscous gear and planet carrier drag, in addition to pocketing losses due to lubricant squeezing at the gear meshes. Both losses are associated with the movement of bodies or gear teeth through an oil bath, which as argued above is not present in the grease-lubricated Powershift hub. While closed-form expressions for these losses exist in literature [32], they should be applied with caution as they are strictly only valid for Newtonian fluids. However, as numerical and experimental investigations indicate that only at elevated velocities ($n \gg 1000$ rpm) the load-independent gear losses may become significant [33], we call upon the relatively low velocities of the Powershift hub components ($n < 1000$ rpm) to justify the approximations made by application of the aforementioned Newtonian loss model. Furthermore, numerical analyses of lubricated gearboxes based on non-Newtonian CFD simulations [34] indicate that load-independent power losses are substantially smaller for grease-lubricated transmissions than for oil-lubricated transmissions operating at the same conditions.

Setting the submerged height parameter equal to 1 (corresponding to full submergence of the planetary gear set within the lubricant) and assuming laminar flow, the gear losses due to viscous drag can be written as [32]:

$$P_{v,g} = 2\pi \nu b r_0^2 \omega^2 + 0.205 \cdot \pi \rho \nu_k^{0.5} r_0^4 \omega^{2.5} \tag{20}$$

where ν is the dynamic viscosity of the lubricant, b is the width of the gear, r_0 is the outer radius of the gear, ω is the rotational velocity expressed in [rad/s], ρ is the density of the lubricant, and ν_k is the kinematic viscosity of the lubricant. Note that the gear angular velocities depend on the selected gear ratio in the Powershift hub.

The gear pocketing losses – which are only present in the 0.686 ratio – are obtained by multiplication of the entrapped lubricant pressure by the leakage areas, which yields the pocketing force, and by multiplication of the latter with the lubricant escaping velocity, which can be obtained from the continuity equation (see [32]):

$$v_{kl}^{(a)} = \frac{b}{2A_{kl}^{(a)}} \frac{dA_{kl}^{(a)}}{d\theta} \omega \tag{21}$$

where $A_{kl}^{(a)}$ is the l-th leakage area of the k-th gear at the a-th angular increment, and θ denotes the angular displacement of the gear. Contrary to the analytical approach outlined in [32], the side leakage areas A_{kl} and their derivatives with respect to θ are obtained by numerical integration of the areas between two adjacent tooth flanks in contact, see Figure 6. The entrapped lubricant pressure is determined incrementally by applying Bernouilli's principle:

$$p_{e,kl}^{(a)} = p_{e,kl}^{(a-1)} + \frac{1}{2}\rho \left[\left(v_{e,kl}^{(a-1)} \right)^2 - \left(v_{e,kl}^{(a)} \right)^2 \right] \tag{22}$$

yielding the following expression for the pocketing loss of gear k due to the l-th leakage area at the a-th angular increment:

$$P_{p,kl}^{(a)} = p_{e,kl}^{(a)} A_{e,kl}^{(a)} v_{e,kl}^{(a)} = A_{e,kl}^{(a)} v_{e,kl}^{(a)} \left\{ p_{e,kl}^{(a-1)} + \frac{1}{2}\rho \left[\left(v_{e,kl}^{(a-1)} \right)^2 - \left(v_{e,kl}^{(a)} \right)^2 \right] \right\} \tag{23}$$

The total gear pocketing loss is then obtained by summation of the losses over both gears and over all leakage areas, and by averaging the obtained expression over all considered angular increments:

$$P_{p,g} = \frac{1}{N_a} \sum_{a=1}^{N_a} \left[\sum_{l=1}^{\lceil \varepsilon \rceil} P_{p,1l}^{(a)} + \sum_{l=1}^{\lceil \varepsilon \rceil} P_{p,2l}^{(a)} \right] \tag{24}$$

where N_a denotes the number of angular increments, ε is the total contact ratio, and $\lceil \cdot \rceil$ denotes the ceiling operator. The above formula is evaluated for all 12 planet gear meshes (2 gear contacts per planet).

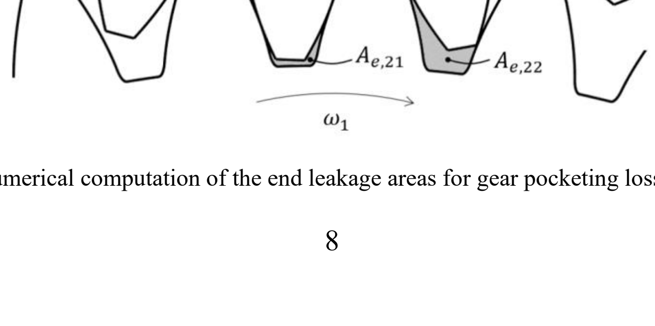

Figure 6. Numerical computation of the end leakage areas for gear pocketing loss computation

Load-independent losses in bearings. Load-independent losses for lubricated bearings consists of viscous drag losses caused by the rolling elements moving through the lubricant, and seal losses that are due to the relative motion between the seal and the inner and/or outer ring(s) of the bearing. For the former, the SKF friction model [25] gives the following expressions for drag losses in ball bearing (main bearings of the Powershift hub) and roller bearings (planet bearings in the hub):

$$P_{v,b}^{m} = 0.04 V_M K_{ball} d_m^5 n^3 \times 10^{-3} \qquad P_{v,b}^{p} = 0.4 V_M K_{roll} C_w B d_m^4 n^3 \times 10^{-3} \tag{25}$$

where B is the width of the rollers and the rolling element constants are

$$K_{ball} = \frac{K_Z(d+D)}{D-d} \times 10^{-12} \qquad K_{roll} = \frac{K_L K_Z(d+D)}{D-d} \times 10^{-12} \tag{26}$$

and where V_M is the drag loss factor and C_w, K_Z and K_L are constants related to the bearing geometry as determined in [25].

Finally, the power loss due to seal friction is essentially proportional to the seal counter face diameter d_s and can be obtained using the following semi-empirical expression [25]:

$$P_{s,b} = \left[K_{S1} d_s^{\beta} + K_{S2}\right] \omega \tag{27}$$

where all constants depend on the seal type and bearing type. Note that only the main bearings of the Powershift hub have seals, with the planet bearings operating without seals.

A final loss factor that should be taken into account are the losses in the one-way bearing supporting the sun gear. The one-way bearing is of the roller ramp clutch type [35] and operates in the free-wheel configuration when the Powershift hub is in the 1:1 ratio. In this configuration, a spring acting on the rollers' cage ensures that the rollers remain in contact with the outer raceway (the inner bore of the sun gear). When in the 0.686 ratio the rollers are forced up the ramps such that they lock the sun gear in place and thereby establish torque transfer between the sun and the axle. In this case there are no losses in the one-way bearing. For the calculation of the losses in the one-way bearing in the 1:1 ratio, a condition of pure sliding is considered as a worst-case estimate, where the rollers remain stationary with respect to the axle and pure sliding occurs between the rollers and inner bore of the sun gear. The torque loss due to sliding friction S_b^{owb} in this case can be obtained as follows:

$$S_b^{owb} = N_{owb} \mu F_{N,s} (d_{s,i}/2) \omega_s \tag{28}$$

where N_{owb} is the number of rollers in the one-way bearing, μ is the friction coefficient for the roller-sun gear contacts (taken as $\mu = 0.0022$ according to [36]), $F_{N,s}$ is the normal force between roller and sun gear exerted by the cage spring, $d_{s,i}$ is the inner diameter of the sun gear, and ω_s is the sun gear's rotational velocity. Note that while sliding friction is considered as a load-independent loss, the sun gear carries no torque in the 1:1 ratio and the only force dependency comes from the spring force, which does not depend on the torque exerted on the Powershift hub. The force $F_{N,s}$ is a function of the ramp geometry and the stiffness constant of the spring.

In summary, the load-independent power losses of the Powershift hub can be summarized as follows:

$$P_{nf} = P_{v,g} + P_{p,g} + P_{v,b} + P_{s,b} + S_b^{owb} \tag{29}$$

Note that in the 1:1 ratio, no gear pocketing losses nor planet bearing drag losses are present, with only three of the four main bearings contributing to the overall seal losses. In the 0.686 ratio, instead, the four main bearings contribute to the overall seal losses, with three of those bearings running at lower speeds. The sliding friction losses in the one-way bearing S_b^{owb} are only present in the 1:1 ratio, acting as a fourth bearing but without any radial load as the sun gear is centered within the planets.

3.3 Numerical simulation of the Powershift hub efficiency

The power losses in the Powershift hub are computed using Eq. 10-29, depending on the selected ratio. In the 0.686 ratio the power losses depend on the angular configuration of the planetary gear set inside the hub. Hence the reported power losses below are obtained by averaging the power losses over one meshing period of the planetary gear set, which for the specific topology employed in the Powershift hub can be obtained as

$$\Delta\theta_{mesh} = \frac{2\pi}{N_p}\frac{z_r + z_s}{z_r z_s} \tag{30}$$

In the 1:1 ratio none of the epicyclic gears rotate with respect to each other; hence no gear meshing losses occur and a single power loss computation suffices. Note that in this ratio, the only losses that are taken into account are the main bearing losses (Eq. 14-18 for the load-dependent and Eq. 25-27 for the load-independent losses) the viscous drag losses due to the gear set motion (Eq. 20) and the sliding friction losses in the one-way bearing (Eq. 28). In the 0.686 ratio, instead, all losses discussed in the previous sections are included, besides the one-way bearing losses.

The power loss equations (Eq. 10-29) depend on a large number of model parameters. As the gear losses are largely obtained from first-principles physics models, the associated parameters could readily be obtained from the gear geometries and the technical data of the applied lubricant. The bearing loss models, instead, are largely empirical models and are expressed in terms of parameters that depend on the bearing type, the number of rolling elements and the bearing geometry (see [25]). The main bearings of the Powershift hub are deep-groove ball bearings with dimensions 17x26x5, 17x28x7, 18x30x7 and 35x44x5 (all expressed in mm), the latter being the bearing that is short-circuited in the 1:1 ratio and does not contribute to the overall bearing losses.

A breakdown of the total predicted power loss in the Powershift hub for a cyclist outputting 300 watts of power and riding at a ground velocity of 30 km per hour in the 0.686 ratio is shown in Figure 7. At this power, approximately 2.5 watts of power are lost due to dissipative effects in the hub, leading to a transmission efficiency of 99.17%. It is important to note that this power loss analysis was carried out for a weightless cyclist, in order for the results to be comparable with the efficiency measurements (see next two sections). When weight is added, the radial forces acting on the bearings will increase, leading to increased load-dependent losses. The influence of weight on the overall hub efficiency is shown for the same operating conditions (300 watts of input power and 30 km per hour in the 0.686 ratio) in Figure 8, where a reduction of 0.12% in efficiency can be observed at a combined weight of bike and rider of 80 kg due mainly to the increased load-dependent losses in the main bearings. Note that these weight dependent losses apply for both the 0.686 and 1:1 ratios.

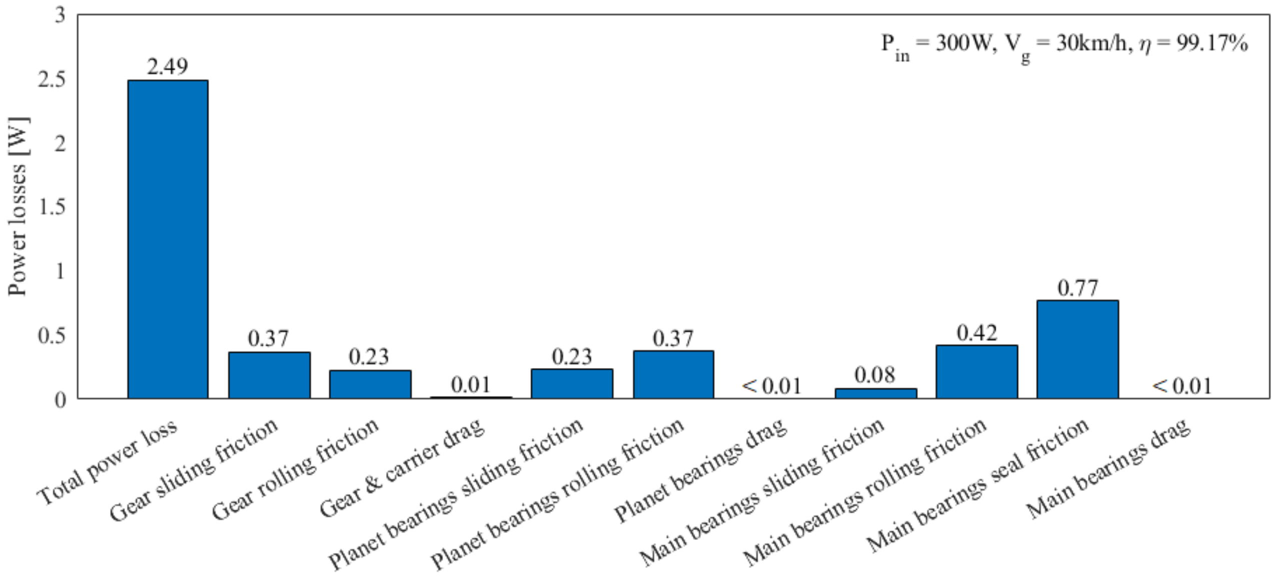

Figure 7. Breakdown of total power loss in the 0.686 ratio at 300 watts of input power and ground speed of 30 km/h

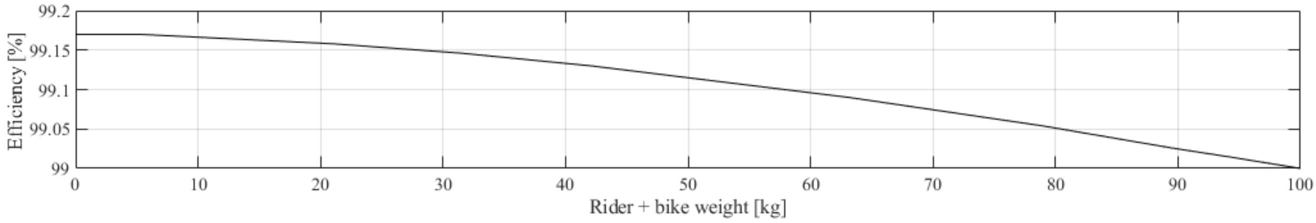

Figure 8. Efficiency in function of weight for the same operating conditions as in Figure 7

In the conditions analyzed in Figure 7, the load-dependent losses amount to 1.7 watts or 68% of the total power losses, whereas the load-independent losses make up 0.78 watts or 32% of the total losses. In Figure 9 and Figure 10 the load-dependent and load-independent losses are shown in function of torque, speed and power for the Powershift hub in the 0.686 ratio. It is evident from these figures that the load-dependent losses increase with the applied power or torque, whereas the load-independent losses are constant for varying torque yet are proportional to the ground velocity of the bicycle. This translates into varying efficiencies depending on the applied power and ground velocity of the bicycle, as can be seen in Figure 11. Note here that the Powershift hub is most efficient when power is high and speed is low: predicted efficiencies of 99.5% and above are observed at these operating conditions, which are characteristic of steep hill climbing in e.g. road and mountain biking. Finally, simulations in the 0.686 ratio were carried out until ground speeds of 35 km/h; beyond these speeds the pedaling efficiency rather than drivetrain efficiency becomes the limiting factor for cycling performance.

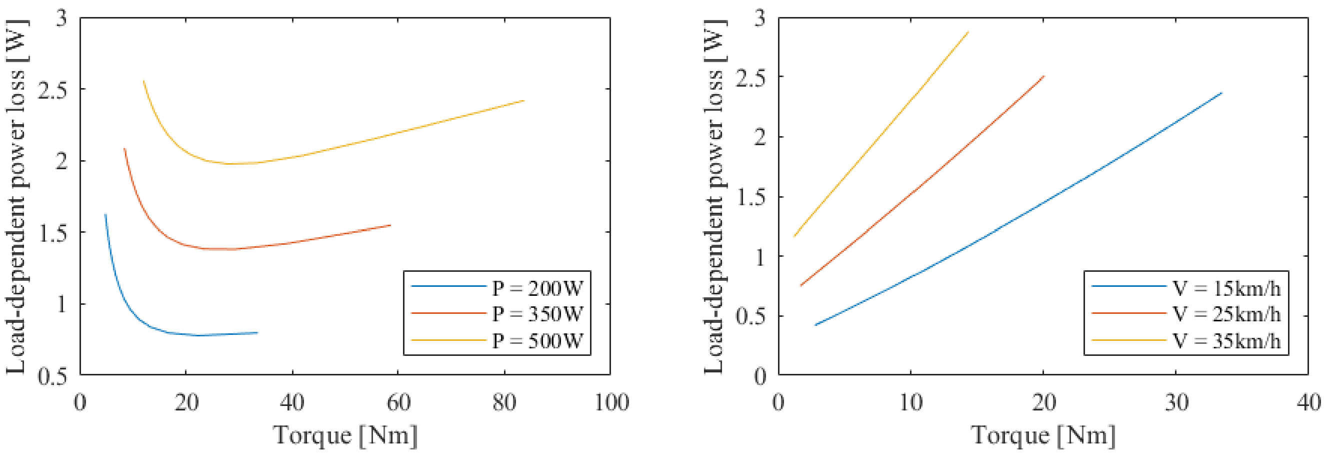

Figure 9. Load-dependent losses in the Powershift hub in the 0.686 ratio as a function of torque, power and speed

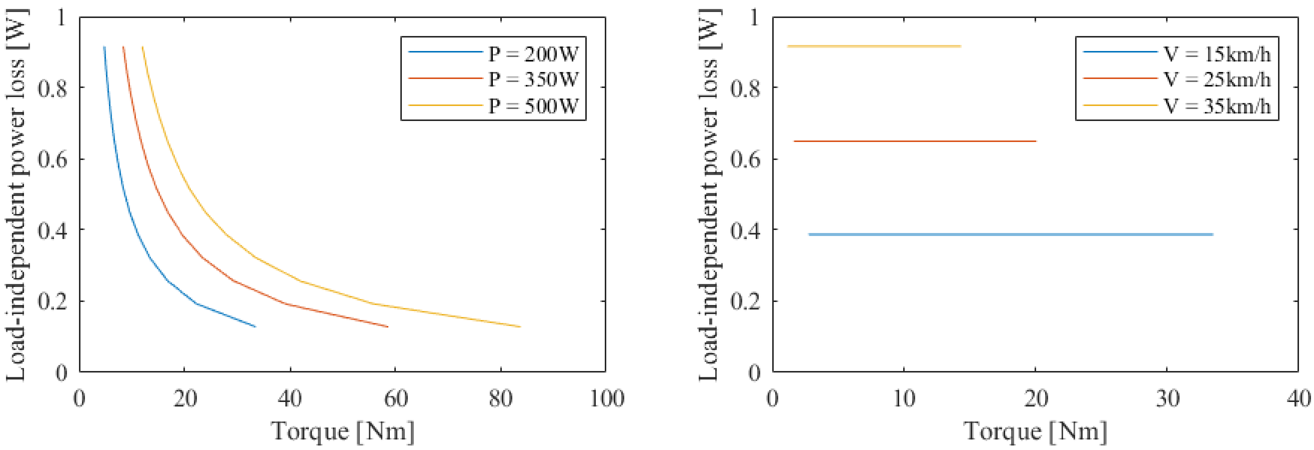

Figure 10. Load-independent losses in the Powershift hub in the 0.686 ratio as a function of torque, power and speed

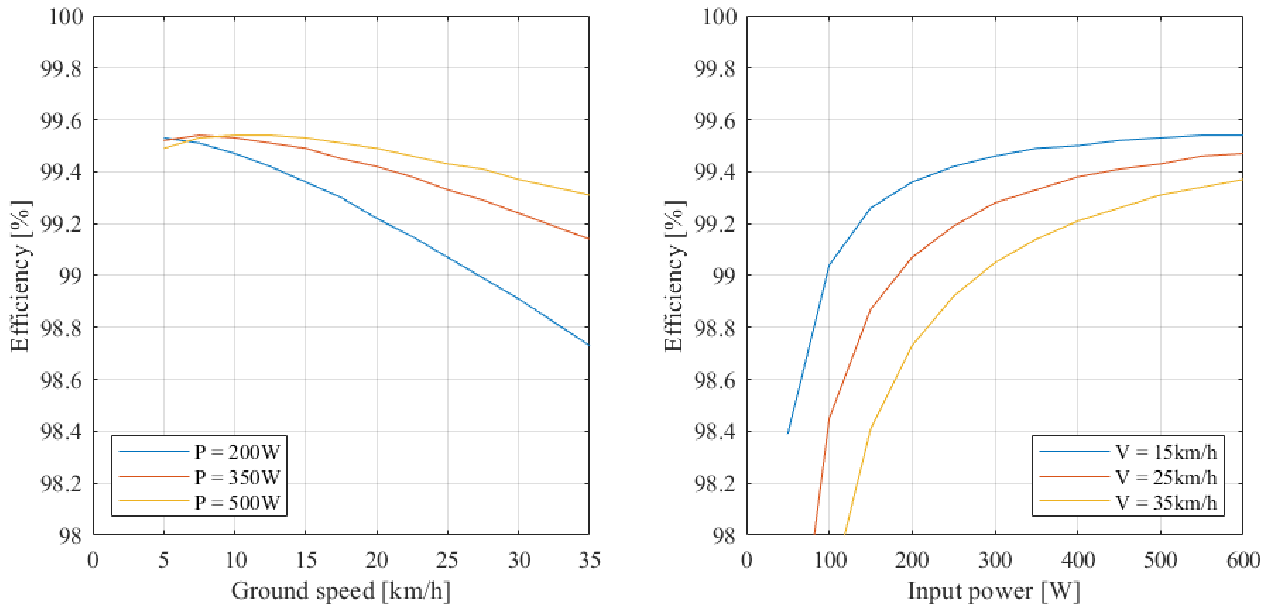

Figure 11. Predicted efficiency of the Powershift hub in the 0.686 ratio as a function of input power and ground speed

When used in the 1:1 ratio, the planetary gear stage of the Powershift hub is not engaged yet rotates as a single unit without relative motion between the ring gear (~cassette) and planet carrier (~rear wheel). The only losses present in this ratio are three of the four main bearing losses, the one-way bearing losses, and the gear and planet carrier drag losses due to synchronous rotation of the planetary gear stage, the latter being negligibly small. This can be observed in Figure 12, that shows a breakdown of the total power loss of the Powershift hub in the 1:1 ratio at the same input power and speed as in Figure 7. Note that the bearing seal losses in this ratio are considerably smaller than the seal losses in the 0.686 ratio, which is due to the fact that the largest of the main bearings of the hub is short-circuited and hence does not contribute to the overall losses. The predicted efficiency of the drivetrain at these conditions is 99.83%, with higher efficiencies being reached at higher input powers, as can be seen in Figure 13. While as for the 0.686 ratio the hub efficiency slightly drops with increasing speed at constant power, the power loss in the 1:1 at elevated speeds becomes negligible. For example, when sprints in road cycling are contested at ground speeds of 60 km per hour and crank powers of 1000 watts and more, the efficiency of the Powershift hub surpasses 99.9%. As for the 0.686 ratio, efficiency is maximal for high powers and low speeds. The efficiency maps of the Powershift hub are shown for the 0.686 and 1:1 ratios in Figure 14.

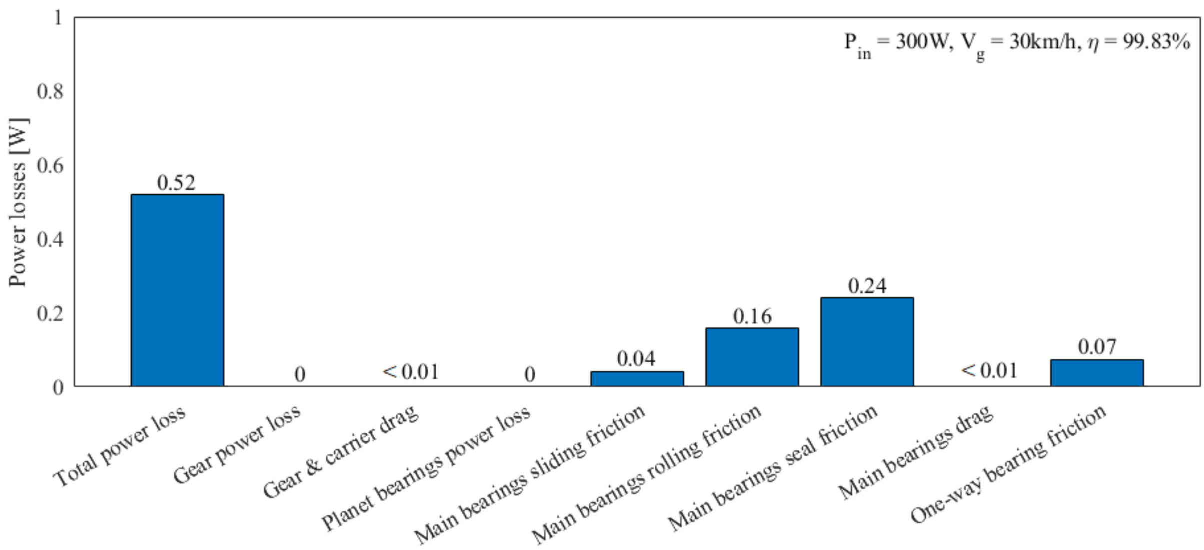

Figure 12. Breakdown of total power loss in the 1:1 ratio at 300 watts of input power and ground speed of 30 km/h

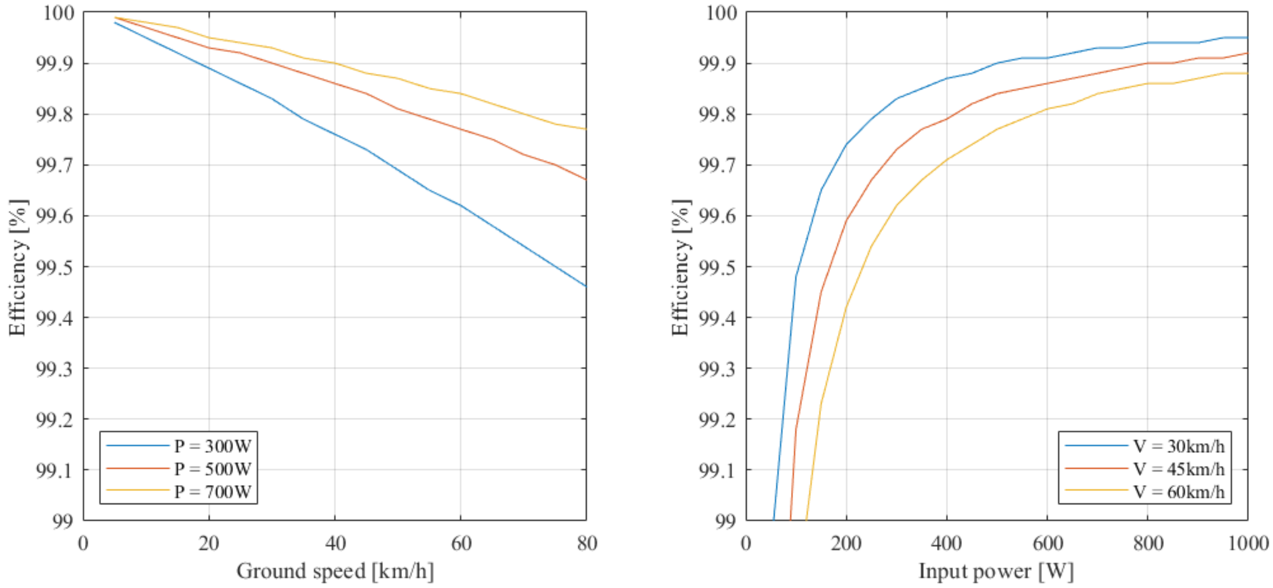

Figure 13. Predicted efficiency of the Powershift hub in the 1:1 ratio in function of input power and ground speed

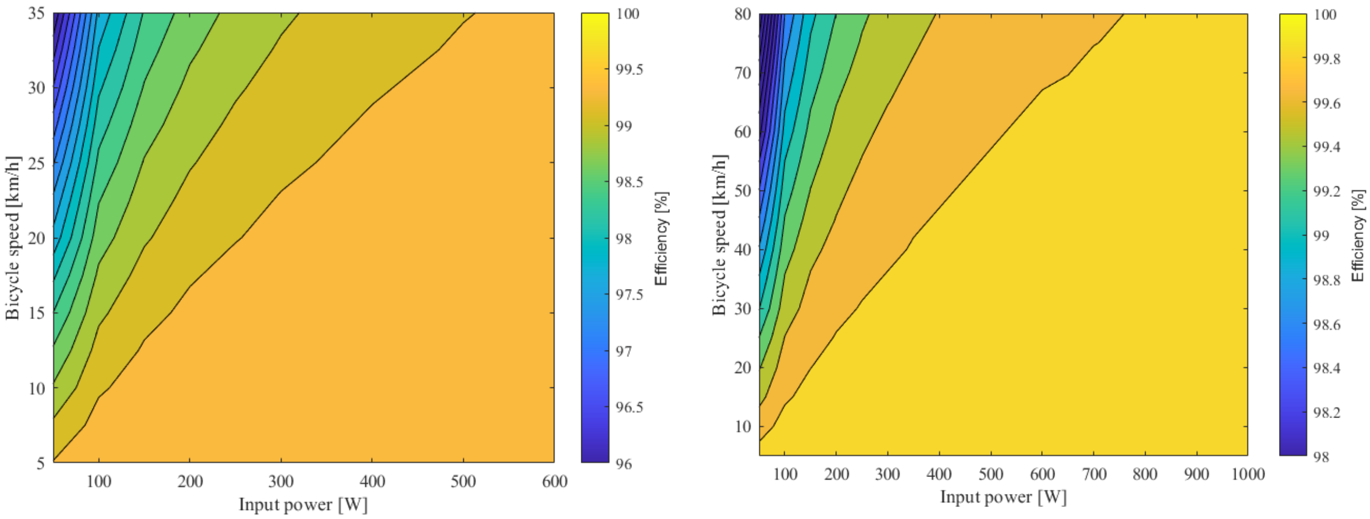

Figure 14. Efficiency maps of the Powershift hub in the 0.686 (left) and 1:1 ratios

4. Accuracy of the efficiency measurement test rig

In order to accurately measure the efficiency of its Powershift hubs, Classified Cycling has acquired custom-built test infrastructure that was designed and constructed by Mevi Engineering in The Netherlands. The infrastructure can be used in two configurations: either as a drivetrain efficiency tester that measures the power losses of the whole drivetrain, including the hub, cassette, chain, chainring and bottom bracket losses, or as a hub efficiency tester, which is the configuration that is of interest in this article. A picture of the hub efficiency tester is shown in Figure 15. The tester consists of two sides: the drive side represents the input torque and speed applied to the ring gear via the cassette and chain, and the hub side represents the output torque and speed applied to the bicycle's rear wheel via the planet carrier and hub shell (see Figure 1). Both drive and hub sides are equipped with a direct drive brushless motor with low inertia and cogging torque and with an integrated Hall sensor for angular velocity measurements. The torque exerted by each motor is measured by a load cell that tangentially supports the stator and absorbs the majority of the stator's reaction torque. The reason for using load cells rather than a torque sensors is because this configuration allows to cancel out stator bearing losses in both ratios without the introduction of additional sensor bearings. Note that in this test rig configuration, no external radial or axial loads can be applied to the Powershift hub. This mostly affects the load-dependent losses in the main bearings of the hub, which in reality support the weight of the rider, the chain tension and any axial forces that are due to the lateral dynamics of the bicycle. The influence of these forces on the bearing losses has been investigated numerically in the previous section.

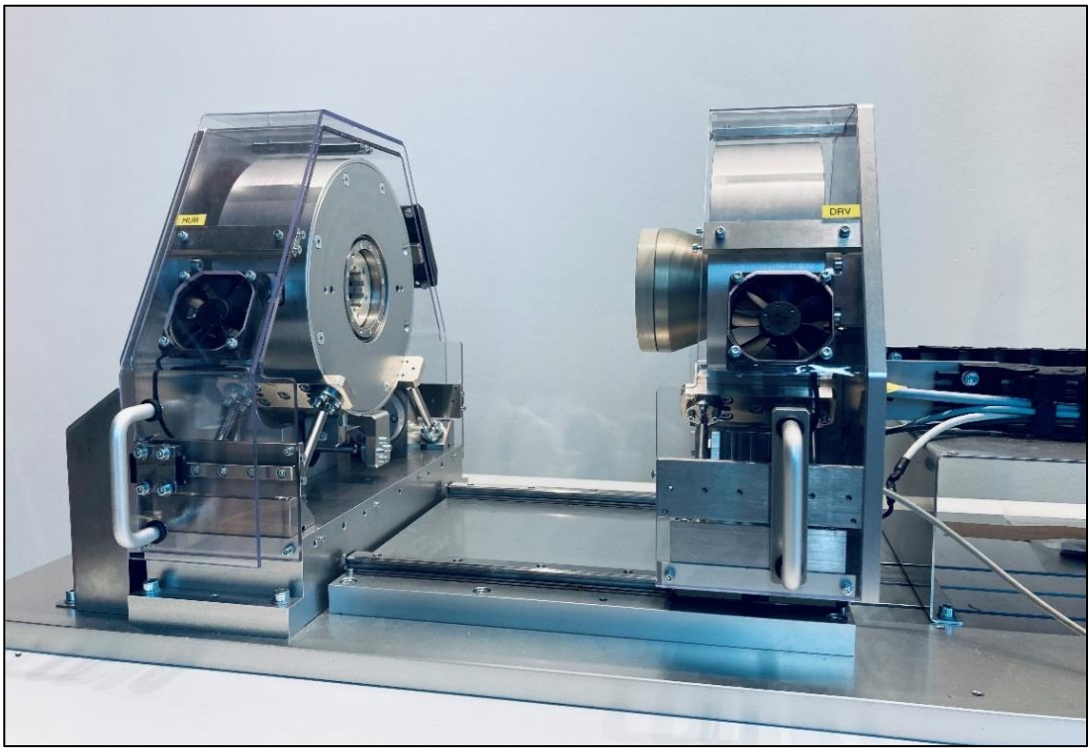

Figure 15. The efficiency test rig infrastructure in the isolated hub configuration

The Powershift hub efficiency is measured by dividing the output ("hub side") power by the input ("drive side") power, where power is obtained by multiplication of the measured torque and angular velocity:

$$\eta = \frac{P_{out}}{P_{in}} = \frac{T_{out}\omega_{out}}{T_{in}\omega_{in}} \tag{31}$$

The accuracy of this measurement is dependent on the accuracy of the individual measurements constituting the efficiency measurement, i.e. the two torque and velocity measurements. For a physical quantity y obtained by measuring n independent quantities x_i

$$y = f(x_1, x_2, \dots, x_n) \tag{32}$$

The absolute maximum error Δy can be calculated from the n individual absolute errors Δx_i as follows [37]:

$$\Delta y = \pm \sum_{i=1}^{n} \left|\frac{\partial f}{\partial x_i}\right| \Delta x_i \tag{33}$$

Applying this formula to Eq. 31 yields the following expressions for the absolute and relative errors of the efficiency measurement:

$$\Delta\eta = \pm\left(\eta\frac{\Delta T_{out}}{T_{out}} + \eta\frac{\Delta\omega_{out}}{\omega_{out}} + \eta\frac{\Delta T_{in}}{T_{in}} + \eta\frac{\Delta\omega_{in}}{\omega_{in}}\right), \quad \frac{\Delta\eta}{\eta} = \pm\left(\frac{\Delta T_{out}}{T_{out}} + \frac{\Delta\omega_{out}}{\omega_{out}} + \frac{\Delta T_{in}}{T_{in}} + \frac{\Delta\omega_{in}}{\omega_{in}}\right) \tag{34}$$

In the efficiency tester, the absolute errors of the torque measurement consist of three main errors: errors due to load cell nonlinearity, structural errors due to dimensional tolerances and parasitic suspension errors in the load cell reading, and discretization errors due to the conversion of analog to digital signals. Table 1 lists the various error sources with their absolute and/or relative error(s). Based on this table, the relative error on the torque measurement is

$$\frac{\Delta T}{T} = \pm\left(\frac{0.00036}{T} + 0.0006\right) \times 100\ [\%] \tag{35}$$

Speed is measured by a rotary encoder integrated into the motor housing using hall sensors with a resolution of 6 times the number of pole pairs (= 8) per revolution, yielding 196 pulses per revolution using quadrature encoding. As the encoder operates based on a frequency measurement approach [38], the relative error on the speed measurement is

$$\frac{\Delta\omega}{\omega} = \pm\frac{2\pi}{\omega N_{ppr} T_{pc}} \times 100\ [\%] \tag{36}$$

where N_{ppr} is the number of pulses per revolution and T_{pc} is the constant-width time window in which the number of pulses are counted. As controller bandwidth is not critical in the steady-state efficiency measurements that are targeted, the error on speed measurement is reduced by increasing T_{pc} and applying filtering based on moving averages. In doing so, the overall relative error on the efficiency measurement can be written as:

$$\frac{\Delta\eta}{\eta} \approx \pm\left(\frac{0.00036}{T_{in}} + \frac{0.0015}{\omega_{in}} + \frac{0.00036}{T_{out}} + \frac{0.0015}{\omega_{out}} + 0.0012\right) \times 100\ [\%] \tag{37}$$

This relative error in the 0.686 ratio is plotted in Figure 16 for the range of torques and speeds considered in this article. At 15 Nm of input torques and an input speed of 300 rpm, the error is $\pm 0.12\%$. Note that this is the maximum error of the efficiency measurement. With the nonlinearity error on the load cell being largest at the extremities of the load cell range, and the dimensional and analog-to-digital conversion errors following a normal distribution, one may expect considerably smaller errors on repeated measurements in practice.

Error source	**Absolute error**	**Relative error**
Non-linearity error on the load cell reading	/	± 0.03%
Temperature error in the nominal temperature range	/	$\ll$ 0.001%
Parasitic suspension error on the load cell reading	/	± 0.005%
Dimensional error on the load cell moment arm	/	± 0.025%
Analog-to-digital conversion (16 bit, $\pm$24 Nm)	± 0.36 Nmm	± 0.00076% F.S.

Table 1. Quantification of maximal errors on torque measurement.

As a sanity check for the accuracy of the efficiency measurement, a dummy Powershift hub was designed and 3D printed (left side of Figure 17) to directly link the drive and the hub side of the efficiency test rig, leading to a theoretical efficiency of 100% (neglecting the miniscule losses due to dissipative effects in the dummy hub). As can be observed from the right side of Figure 17, the efficiency test rig measured close to 100% efficiency under all investigated operating conditions (99.98-99.99%). One may also appreciate from these measurements that the theoretical error bounds on the measurement (Eq. 37) represent a worst-case situation which in practice will rarely be met.

Finally, in order to investigate the repeatability of the efficiency measurements, all measurements were repeated 5 times and the spread on the obtained measurements was assessed. In Figure 18 it can be seen that the spread on efficiency measurements in the 0.686 ratio remains consistently below 0.05%, proving the repeatability of the test rig and test procedure.

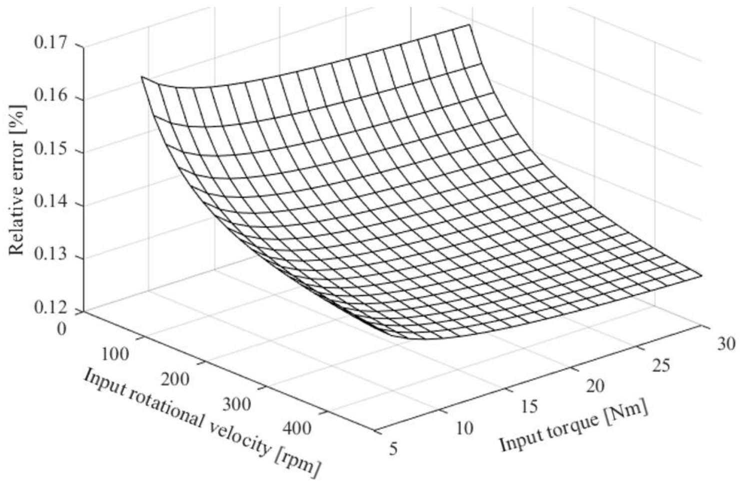

Figure 16. Relative error of the efficiency measurement in function of input torque and speed


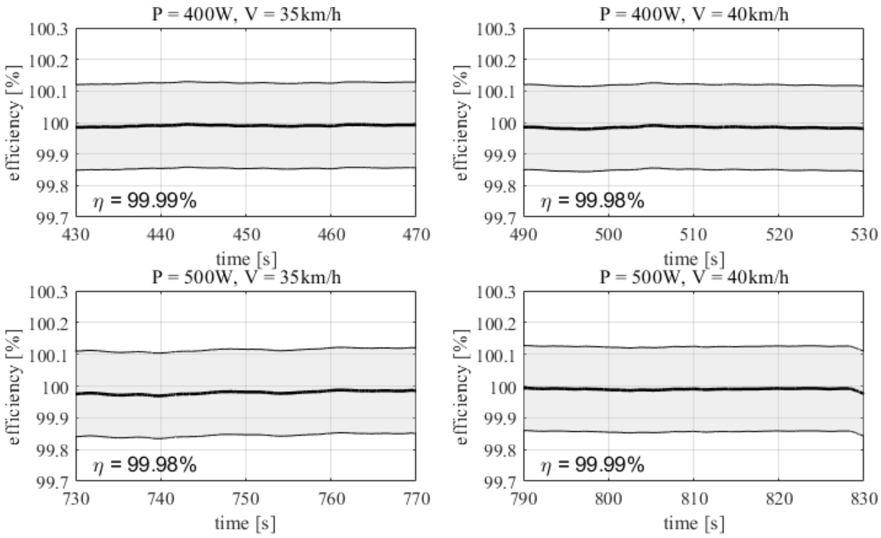

Figure 17. Dummy Powershift hub and measurements used to verify the efficiency test rig at 100% theoretical efficiency

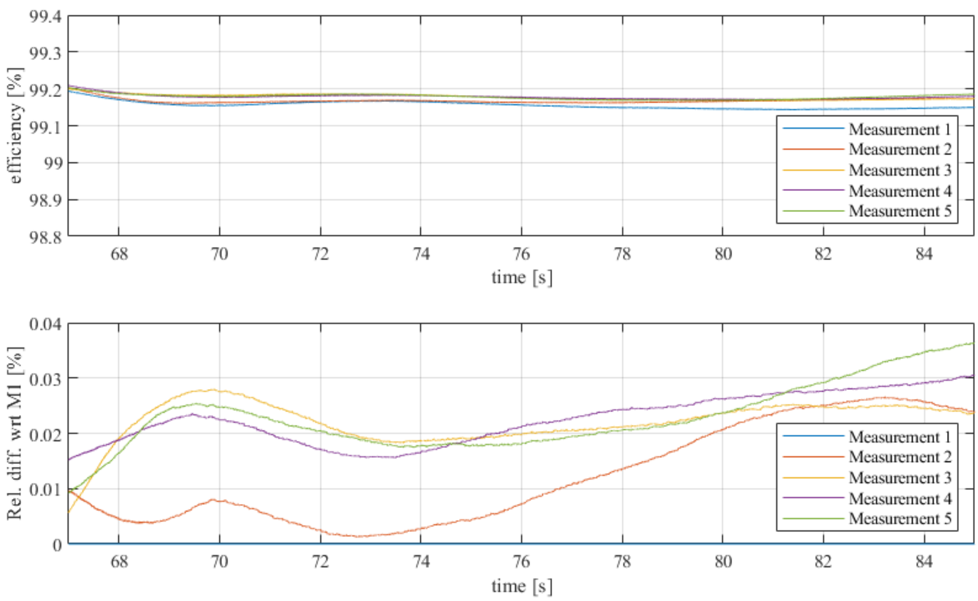

Figure 18. Variation of the efficiency measurements over repeated tests in the 0.686 ratio (top) and relative difference in measured efficiency with respect to the first measurement (bottom)

5. Efficiency measurements of the Powershift hub

The efficiency measurements conducted to assess the efficiency of the Powershift hub are performed at a constant input torque and speed. While in reality the input speed of the hub within a bicycle is indeed relatively constant, the torque supplied by the cyclist is widely variable with variations of 90% and more throughout a single crank revolution [39]. Some researchers have suggested that the torque level in constant-torque efficiency measurements should be set equal to the maximal torque, as this is the torque level at which laboratory wear measurements optimally correlate with in-field observations [9]. However, this approach leads to overestimation of the actual efficiency, as the efficiency of any geared transmission tends to increase with torque (see Section 3). Therefore average torque was applied in the presented measurements, where based on ground velocity V_g [m/s] and crank power P_{crank} [W], the input velocity n_{in} [rpm] and input torque T_{in} [Nm] applied to the Powershift hub are obtained as follows:

$$n_{in} = \frac{60}{\pi}\frac{V_g}{d_w}\frac{1}{u_{PS}} \qquad\qquad T_{in} = \frac{P_{crank} d_w u_{PS}}{2V_g} \tag{38}$$

where d_w is the sum of the wheel and the tire diameter, and u_{PS} is the selected Powershift ratio (1 or 0.686). In order to not overload the motors of the efficiency tester, current tests were conducted at maximal powers of 400W in the 0.686 ratio and 500W in the 1:1 ratio. All measurements were performed on hubs that had just left the factory (see Figure 19). Like any other Powershift hub, the tested hubs had undergone end-of-line testing, which consists of a 3 min long test in which multiple consecutive shifts are executed while verifying the proper functioning of the hub. While this test initiates optimal spreading of the applied grease, it is not sufficiently long to investigate the influence of extended running-in periods, which are known to favor the efficiency of greased transmissions [25]. Measurement results for the 0.686 ratio and 1:1 ratio are shown in Figure 20 and Figure 21, respectively. In each graph, the measurement is represented by a solid black line, the accuracy interval taking into account Eq. 37 is marked in light gray, and the efficiency predicted by the numerical model described in Section 3 is depicted as a dashed blue line.

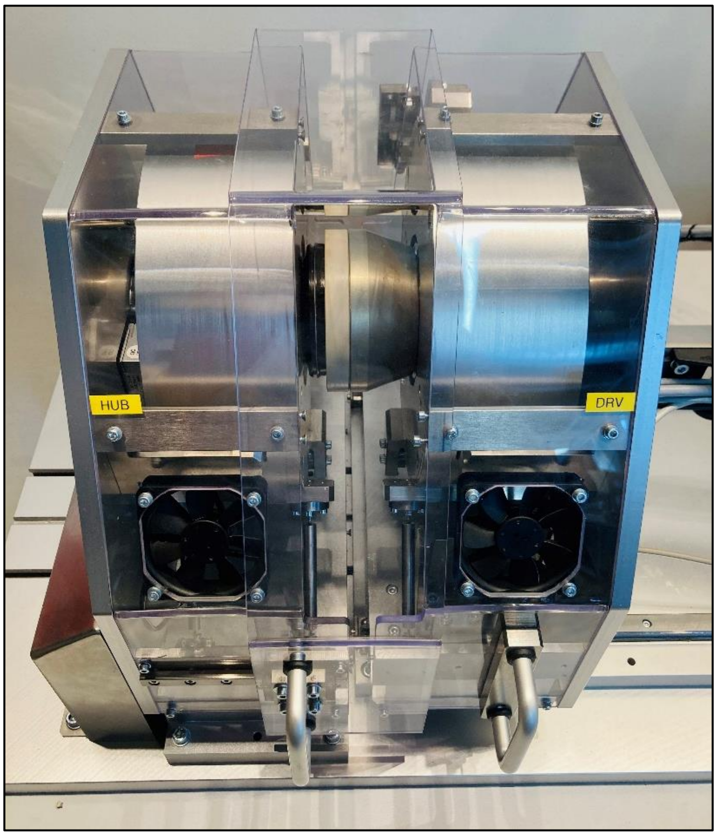

Figure 19. The Powershift hub mounted in the efficiency test rig during end-of-line testing and efficiency measurement

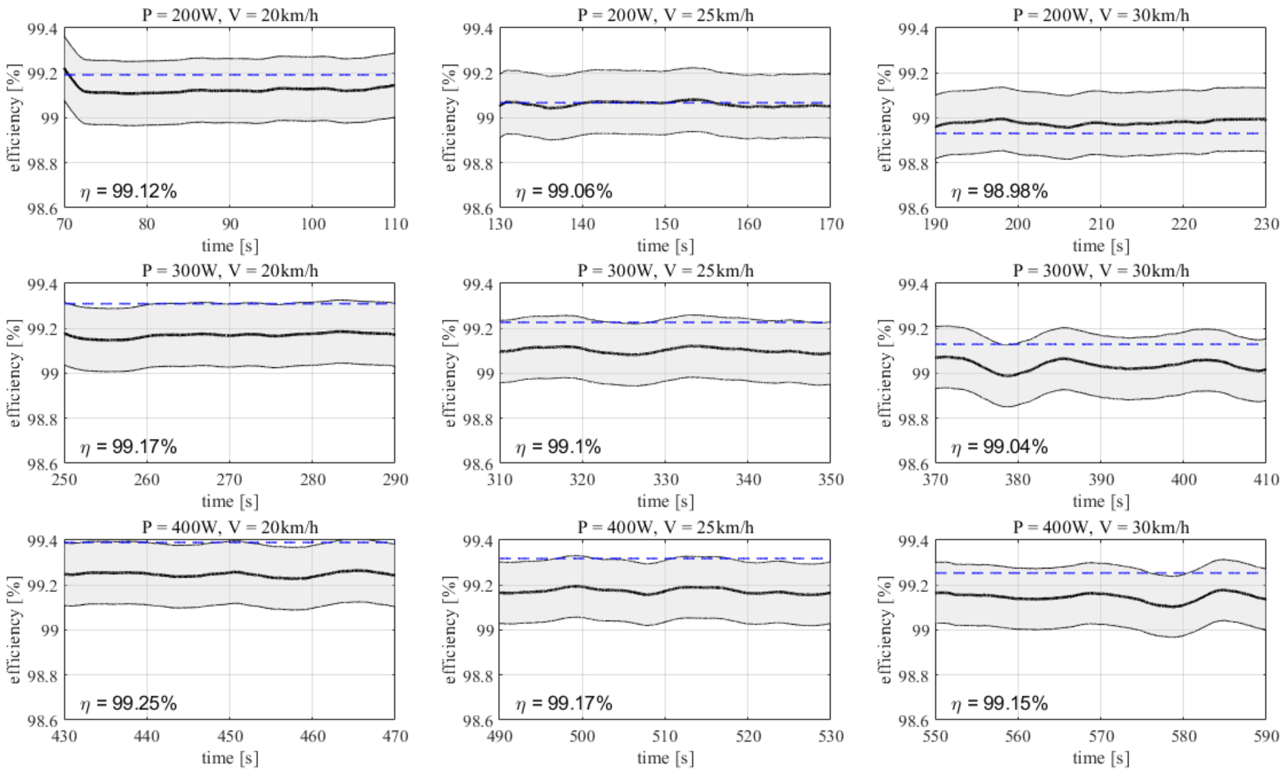

Figure 20. Efficiency measurements at various powers and speeds in the 0.686 ratio. Solid black line shows measured efficiency, with error interval indicated in gray and mean value summarized in bottom left corner. Dashed blue line shows predicted efficiency.

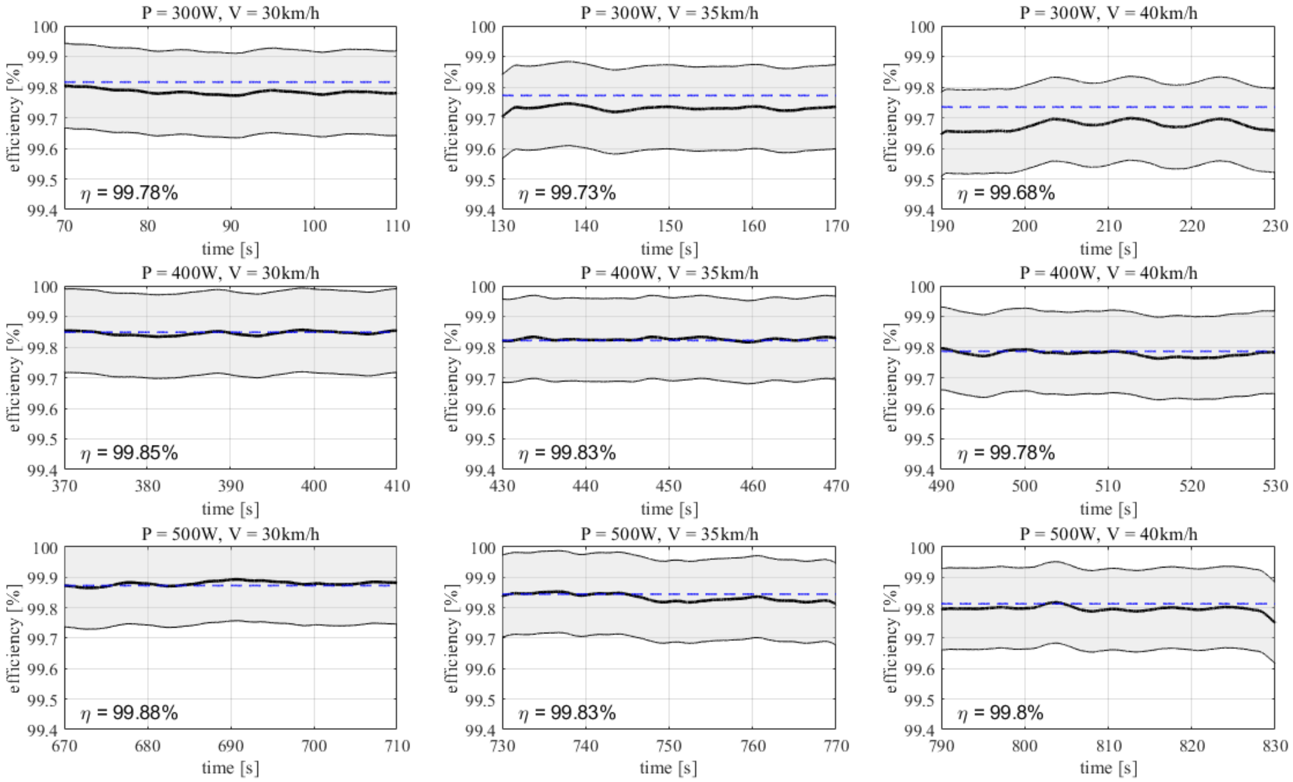

Figure 21. Efficiency measurements at various powers and speeds in the 1:1 ratio. Solid black line shows measured efficiency, with error interval indicated in gray and mean value summarized in bottom left corner. Dashed blue line shows predicted efficiency.

The results in Figure 20 and Figure 21 show that the efficiency measurements are in line with the efficiency predictions discussed in Section 3, in the sense that in general the predicted hub efficiency falls within the error bounds of the measurement. Note that for the efficiency predictions, all parameters of the power loss equations (Eq. 10-29) were taken from catalogs, technical sheets and literature at face value, without parameter identification based on efficiency measurements. Needless to say, better agreement between prediction and measurement could be obtained by updating a subset of parameters (e.g. friction coefficients) based on the measurements, yet in the current work this would beat the purpose of the analysis. In the 0.686 ratio, efficiencies between 99.04% and 99.25% were measured for power varying between 200W and 400W and ground speeds varying between 20 km/h and 30km/h. In the 1:1 ratio, efficiencies between 99.68% and 99.88% were measured for power varying between 300W and 500W and speeds varying between 30km/h and 40km/h. Note that at higher input torque (~power), the efficiency of the Powershift hub should increase even further (see Section 3).

To put the efficiency of the Powershift hub in the 1:1 ratio in perspective, it is compared to the efficiency of a popular conventional race bike hub, namely the DT Swiss 240 rear hub. In order to measure the efficiency of this hub using the efficiency test rig discussed above, a number of custom components were 3D printed to mount the hub on the rig and provide realistic support conditions (see Figure 22). Note that, as in the case of the Powershift hub, the components are connected to elastic couplings inside the rotors of the input and output motors so as to ensure misalignments do not affect the efficiency measurements. The same test protocol as in Figure 21 was used to measure the DT Swiss 240 hub efficiency, with the results shown in Figure 23. Prior to the DT Swiss hub measurements, a 20-minute running-in test sequence was ran to make sure the lubricant was properly distributed within the hub. By comparison of the efficiency results of Figure 21 (Powershift hub in the 1:1 ratio) and Figure 23 (DT Swiss 240 hub), one can observe that the efficiencies of these hubs are largely equal, with absolute differences in efficiency of well below 0.1% across all considered operating conditions.

Figure 22. Mounting of a DT Swiss 240 hub in the efficiency test rig using a number of 3D printed components including internal splines on both ends to connect the hub with the flexible couplings inside the input and output motors

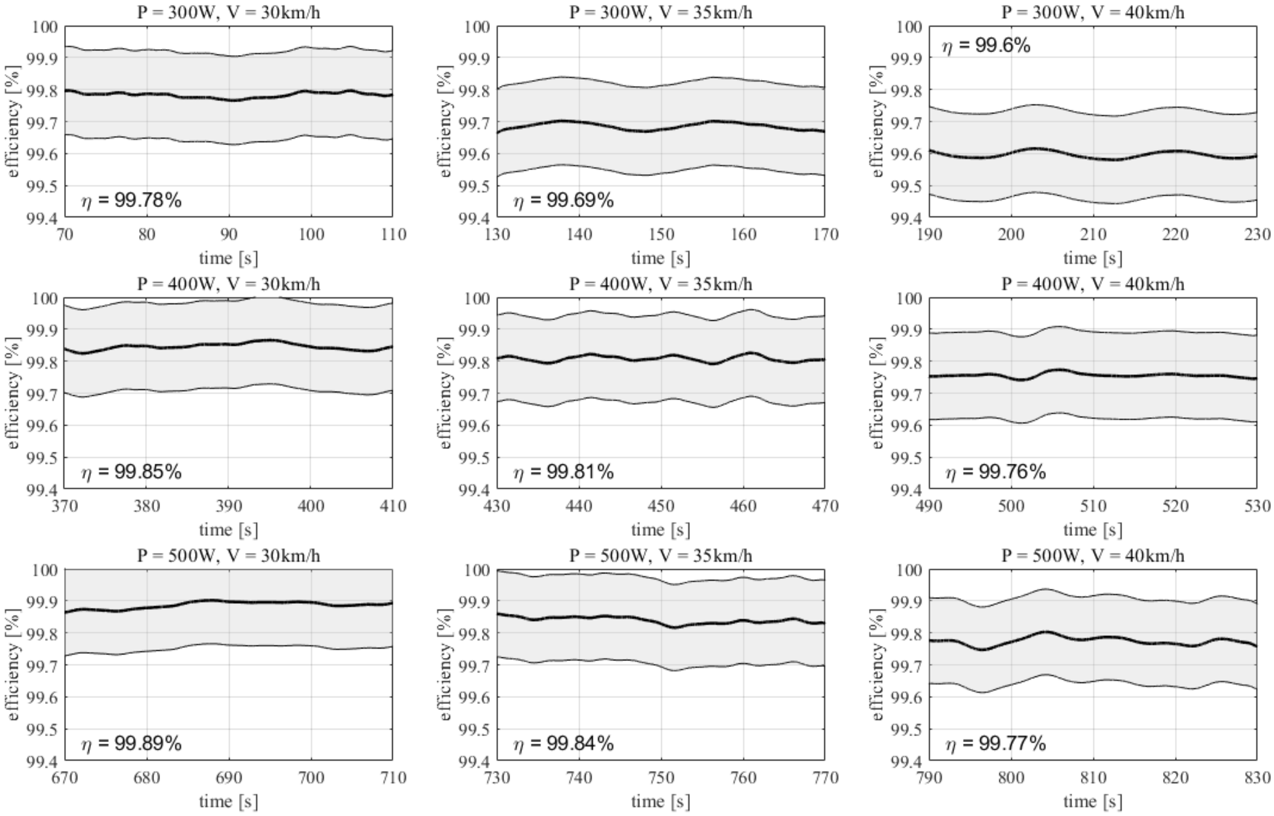

Figure 23. Efficiency measurements at various powers and speeds of the DT Swiss 240 hub. Solid black line shows measured efficiency, with error interval indicated in gray and mean value summarized in bottom left corner.

6. Conclusion and outlook

In this article, a theoretical, numerical and experimental analysis of the transmission efficiency of Classified Cycling's Powershift hub technology is presented. The Powershift hub consists of a single-stage epicyclic gearing system that can be operated in two ratios: in the 1:1 ratio the planetary gear stage rotates as a single unit with no relative motion between the various components, whereas in the 0.686 ratio the ring gear, planet carrier and planet gears rotate at different angular velocities while the planet gears mesh with the ring gear and the stationary sun gear. This particular epicyclic configuration yields a theoretical efficiency of 99.5% and above for realistic equivalent coefficients of friction. A detailed numerical model of the Powershift hub was developed based on a three-dimensional loaded tooth contact analysis, including both load-dependent and load-independent losses in the gears and bearings of the Powershift hub. Numerical predictions of the Powershift hub efficiency confirm the Powershift's theoretical efficiency, as in the 0.686 ratio efficiencies between 99.0 and 99.5% are predicted, and efficiencies in the 1:1 ratio falling between 99.7 and 99.9%. An accuracy analysis of the Powershift efficiency test rig located at Classified Cycling's facilities was conducted and indicated an efficiency measurement error of maximally $\pm$0.16%, with higher accuracies obtained depending on the operating conditions of the test rig. This test rig was then used to conduct efficiency measurements on the isolated Powershift hub, which were shown to be in line with the numerical efficiency predictions: in the 0.686 ratio efficiencies up to 99.25% were measured whereas in the 1:1 ratio efficiencies up to 99.88% were measured. It should be noted that these measurements were conducted at input powers between 300 and 500W, whereas the Powershift hub, like any geared transmission, is known to exhibit higher transmission efficiency at higher powers. Furthermore, it was shown that the efficiency of the Powershift hub in the 1:1 ratio is equal (within less than 0,1%) to that of high-performant conventional bicycle hubs such as the DT Swiss 240 hub.

References

[1] Talbot, D. C., Kahraman, A., and Singh, A. (February 3, 2012). "An Experimental Investigation of the Efficiency of Planetary Gear Sets." ASME. *J. Mech. Des*. February 2012; 134(2).

[2] Krantz, T. L. (1990). "Experimental and analytical evaluation of efficiency of helicopter planetary stage", No. NASA-TP-3063.

[3] Fernandes, C. M., Blazquez, L., Sanesteban, J., Martins, R. C., & Seabra, J. H. (2016). "Energy efficiency tests in a full scale wind turbine gearbox". Tribology International, 101, 375-382.

[4] Berto, F. (2008) The Dancing Chain: History and Development of the Derailleur Bicycle (3rd ed.). San Francisco, CA, USA: Cycle Publishing/Van der Plas Publications.

[5] Hadland, T. (1987). The Sturmey-Archer Story. Pinkerton Press, Birmingham.

[6] Rohloff, B., Rauch, M. (2010). Rohloff Stories. Rohloff AG.

[7] Kyle, C.R., Berto, F. (2001). "The mechanical efficiency of bicycle derailleur and hub-gear transmissions", Human Power 51.

[8] Casteel, E.A, Archibald, M. "A Study on the Efficiency of Bicycle Hub Gears." Proceedings of the ASME 2013 International Mechanical Engineering Congress and Exposition. Volume 13: Transportation Systems. San Diego, California, USA. November 15–21, 2013.

[9] Rohloff, B., & Greb, P. (2004). "Efficiency measurements of bicycle transmissions - a neverending story?", Human power, 3(8), 20.

[10] Looman, J. (2009). Zahnradgetriebe: Grundlagen, Konstruktionen, Anwendungen in Fahrzeugen. Springer Science & Business Media.

[11] Del Castillo, J. M. (2002). "The analytical expression of the efficiency of planetary gear trains". Mechanism and Machine Theory, 37(2), 197-214.

[12] Pennestri, E., and Freudenstein, F. (1993). "The Mechanical Efficiency of Epicyclic Gear Trains." ASME. J. Mech. Des. September 1993; 115(3): 645–651.

[13] Tuplin, W. A. (1962). Involute gear geometry. F. Unger Publishing Company.

[14] Anderson, N. E., & Loewenthal, S. H. (1983). Comparison of spur gear efficiency prediction methods. Advanced Power Transmission Technol.

[15] Baumann, A., & Bertsche, B. (2022). Coefficient of friction behavior of gear oils and significance for the meshing process of spur gears: Lubrication for improved properties. Forschung im Ingenieurwesen, 1-11.

[16] Talbot, D. C. (2012). An experimental and theoretical investigation of the efficiency of planetary gear sets. The Ohio State University.

[17] Jordan, J. M., Blockmans, B., & Desmet, W. (2023). A linear formulation for misaligned helical gear contact analysis using analytical contact stiffnesses. Mechanism and Machine Theory, 187, 105373.

[18]] Weber, C., Banaschek, K. (1949) "The Deformation of Loaded Gears and the Effect on Their Load Carrying Capacity (Part I)", DSIR, London.

[19] Andersson, A., & Vedmar, L. (2003). A dynamic model to determine vibrations in involute helical gears. Journal of Sound and Vibration, 260(2), 195-212.

[20] ISO, B. 21771 (2007) Gears–Cylindrical Involute Gears and Gear Pairs–Concepts and Geometry. UK: BSI, 1-83.

[21] Blockmans, B. (2018). Model reduction of contact problems in flexible multibody dynamics. PhD dissertation, KU Leuven, Belgium.

[22] Harris, T. A., & Kotzalas, M. N. (2006). Advanced concepts of bearing technology. CRC press.

[23] Liu, H., Liu, H., Zhu, C., & Parker, R. G. (2020). Effects of lubrication on gear performance: A review. Mechanism and Machine Theory, 145, 103701.

[24] Lugt, P. M. (2009). A review on grease lubrication in rolling bearings. Tribology Transactions, 52(4), 470-480.

[25] SKF. Rolling Bearings, PUB BU/P1 10000/2 EN; 2013.

[26] Kanazawa, Y., Sayles, R. S., & Kadiric, A. (2017). Film formation and friction in grease lubricated rolling-sliding non-conformal contacts. Tribology International, 109, 505-518.

[27] Bakolas, V., Roedel, P., Koch, O., & Pausch, M. (2021). A first approximation of the global energy consumption of ball bearings. Tribology Transactions, 64(5), 883-890.

[28] Xu, H., Kahraman, A., Anderson, N. E., & Maddock, D. G. (2007). Prediction of mechanical efficiency of parallel-axis gear pairs. Journal of Mechanical Design, 129(1), 58-68.

[29] Goksem, P. G., and Hargreaves, R. A. (1978). "The Effect of Viscous Shear Heating on Both Film Thickness and Rolling Traction in an EHL Line Contact—Part I: Fully Flooded Conditions." ASME. J. of Lubrication Tech; 100(3): 346–352.

[30] Wu, S., & Cheng, H. S. (1991). A friction model of partial-EHL contacts and its application to power loss in spur gears. Tribology transactions, 34(3), 398-407.
[31] Stacke, L. E., Fritzson, D., & Nordling, P. (1999). BEAST—a rolling bearing simulation tool. Proceedings of the Institution of Mechanical Engineers, Part K: Journal of Multi-body Dynamics, 213(2), 63-71.
[32] Seetharaman, S., and Kahraman, A. (February 26, 2009). "Load-Independent Spin Power Losses of a Spur Gear Pair: Model Formulation." ASME. J. Tribol. April 2009; 131(2): 022201.
[33] Seetharaman, S., Kahraman, A., Moorhead, M. D., and Petry-Johnson, T. T. (February 26, 2009). "Oil Churning Power Losses of a Gear Pair: Experiments and Model Validation." ASME. J. Tribol. April 2009; 131(2): 022202.
[34] Mastrone, M. N., & Concli, F. (2021). CFD simulation of grease lubrication: Analysis of the power losses and lubricant flows inside a back-to-back test rig gearbox. Journal of Non-Newtonian Fluid Mechanics, 297, 104652.
[35] Diirkopp, K., & Jorden, W. (1970). Contact Analysis In Clamping-roller Free-wheel Clutches. WIT Transactions on Engineering Sciences, 1.
[36] SKF. Needle Roller Bearings, PUB PSD/P1 06003/3 EN; 2015.
[37] Pagitsch, M., Jacobs, G., Schelenz, R., Bosse, D., Liewen, C., Reisch, S., & Deicke, M. (2016, September). Feasibility of large-scale calorimetric efficiency measurement for wind turbine generator drivetrains. In Journal of Physics: Conference Series (Vol. 753, No. 7, p. 072011). IOP Publishing.
[38] Petrella, R., Tursini, M., Peretti, L., & Zigliotto, M. (2007, September). Speed measurement algorithms for low-resolution incremental encoder equipped drives: a comparative analysis. In 2007 International Aegean Conference on Electrical Machines and Power Electronics (pp. 780-787). IEEE.
[39] Rosler, K., Conley, K. E., Howald, H. A. N. S., Gerber, C. H. R. I. S. T. I. A. N., & Hoppeler, H. A. N. S. (1986). Specificity of leg power changes to velocities used in bicycle endurance training. Journal of Applied Physiology, 61(1), 30-36.